3
Computational framework for AlGaN/GaN HEMT system

In this chapter, a comprehensive approach to computationally model AlGaN/GaN HEMT devices is presented [Joshi *et al.* 2016]. A detailed account is presented on different physical aspects important for modeling DC behavior of AlGaN/GaN HEMT devices. As discussed in chapter 2, group III-Nitride systems exhibit strong polarization fields resulting in accumulation of polarization charges at different material interfaces. Importance of presence of polarization charges in the AlGaN barrier layer as well as different hetero-interfaces is studied and explained with respect to its impact on conduction band energy and parasitic charges across the epitaxial stack. In order to establish a practical approach for computing behavior of AlGaN/GaN HEMT devices, surface and buffer traps are also considered. Impact of these traps on 2-DEG charge density, device characteristics as well as gate leakage is also taken into account. Moreover, for the first time, a correlation between surface donor trap parameters and gate leakage is established, enabling calculation of surface trap parameters, like concentration and activation energy, from the gate leakage characteristics. In addition to this, a novel approach to accurately model leakage current of Schottky gate, in forward bias condition, is proposed. Finally, impact of self-heating and carrier heating (hot electrons) is studied in conjunction with presence of traps in the device. Furthermore, a strategy to model other important aspects like parasitic charges in the device, presence of quantum confinement effects, Source/Drain contacts and high electric field effects is presented [Joshi *et al.* 2016].

3.1 INTRODUCTION

While AlGaN/GaN HEMT devices are the most favored candidate to replace Silicon based devices in the power semiconductor market and have already shown promising performance figures, yet some bottlenecks in device performance have limited their wide scale deployment. It is essential to adopt a well-developed device design and analysis technique to enable AlGaN/GaN HEMT devices to meet increasing demand for higher efficiency and robustness. For Si based devices, computational modeling-based design approach has proven to be an effective tool to enable performance improvement and reduce time to development for a wide range of applications. Semiconductor industry has widely accepted this approach, as it accurately predicts physics and behavior of complex device designs. Performance improvement and technology development of complex devices, such as FinFET, has greatly benefitted from computational modeling [Shrivastava *et al.* 2008, Shrivastava *et al.* 2010, Shrivastava *et al.* 2012] . Similar approach for Si based power devices, such as LDMOS, has resulted in devices with higher robustness and performance. On the other hand, being part of a relatively emergent technology, GaN based HEMTs lag behind in terms of availability of a well-defined and consistent computational modeling strategy. As a result, the technology development has to rely on experimental results leading to increase in design time and cost. Moreover, the presence of unique polarization effects in group III-N devices combined with presence of traps due to impurities, imperfect interfaces and defects, susceptibility to self-heating and hot-electrons makes it challenging to accurately predict of accurate device behavior of AlGaN/GaN HEMTs.

Computational studies on HEMTs has been discussed in the past [Karmalkar *et al.* 2001, Saito *et al.* 2003, Meneghesso *et al.* 2004b, Palacios *et al.* 2005, Saito *et al.* 2005, Saito *et al.* 2007,

Tirado *et al.* 2007, Bahat-Treidel *et al.* 2008, Faqir *et al.* 2008, Uren *et al.* 2012, Wang *et al.* 2012, Longobardi *et al.* 2014b, Verzellesi *et al.* 2014b], however, a limited set of device aspects are discussed in these works while neglecting other aspects and relevant physics. In order to precisely predict device behavior under different complex boundary conditions which is applicable to different device structures, it is important for the computational framework to encapsulate all relevant physical aspects. With the help of computations, earlier works [Meneghesso *et al.* 2004b, Saito *et al.* 2005, Tirado *et al.* 2007, Faqir *et al.* 2008] have intensively discussed reliability aspects of the device with focus on impact of traps on drain current dispersion [Meneghesso *et al.* 2004b], drain/gate lag effect [Tirado *et al.* 2007], gate leakage, breakdown characteristics [Saito *et al.* 2005] and high field performance of device [Faqir *et al.* 2008]. Karmalkar and Mishra used TCAD simulations to present design guidelines for AlGaN/GaN HEMTs with a field plate connected to gate electrode [Karmalkar *et al.* 2001]. Saito *et al* discussed designing of AlGaN/GaN HEMTs with field plate connected to source electrode with a discussion on breakdown voltage vs. ON-resistance (V_{BD}-R_{ON}) trade-off [Saito *et al.* 2003]. In [Bahat-Treidel *et al.* 2008], Bahat-Treidel *et al* have presented a simulation study which is restricted to assessment of influence of AlGaN, working as a back barrier layer, on conduction band energy across the epitaxial stack and its impact on punch through voltage in HEMT devices based on AlGaN/GaN system. A comprehensive study on source of increase in dynamic source resistance of AlGaN/GaN HEMT devices is presented in [Palacios *et al.* 2005]. Saito *et al* in [Saito *et al.* 2007] analyzed impact of field plate on dynamic-ON resistance of AlGaN/GaN HEMT device, however, the simulations were utilized to gain an insight on the electric field distribution only. Longobardi *et al* limited their simulation study in [Longobardi *et al.* 2014a] to evaluate the impact of donor traps, present on device surface, on sheet charge density and characteristics of AlGaN/GaN HEMTs. A more comprehensive discussion on computation of device characteristics of a double channel HEMT device is presented by Wang et al. in [Wang *et al.* 2012], with discussion on hot electron and self-heating effects in these devices, however, the discussion lacks the important consideration of surface states and traps at other locations which affect device performance. TCAD simulations have also been used to evaluate and predict behavior of doping by agents such as Fe and C in GaN buffer [Uren *et al.* 2012, Verzellesi *et al.* 2014b], which conclude with the observation that these doping agents behave as acceptor trap centers leading to increase in current collapse effect after buffer doping. However, these studies focus specifically on impact of traps in GaN buffer on current collapse phenomena and neglect any role of surface traps and hot electrons which, as will be described later, are essential to model device behavior.

While these earlier computational works provide a reasonable insight into optimization and reliability behavior of device pertaining to a limited aspect of the AlGaN/GaN HEMTs; however, they fail to encapsulate, discuss and present all the physical aspects that are required to accurately capture the device characteristics. In this chapter, all the critical aspects related to operation of AlGaN/GaN HEMT devices are discussed and explained while establishing relevance and capturing critical aspects like polarization charge, surface and bulk traps, quantum effects, Source/Drain contacts, gate stack modeling, gate leakage, carrier tunneling, carrier dynamics, high field effects, hot electrons, and self-heating behavior.

Based on the findings of this work a computational modeling strategy is established. This strategy enables physics-based estimation of experimental trends and electrical characteristics of newer designs. Commercially available Sentaurus TCAD Synopsys (2014) was used for numerical computations. This chapter is arranged as follows. The HEMT device structure considered here with the experimentally measured characteristics is discussed in Section 3.2. Different challenges associated with modelling of physical aspects, impact of physical parameters and proposed modeling approach are discussed collectively in Section 3.3 and 3.4. While electrostatics related aspects are discussed in Section 3.3, a detailed account of the carrier transport related modeling aspects is presented in Section 3.4. Finally, a conclusion of the discussion is presented in section 3.5.

3.2 HEMT DEVICE STRUCTURE AND EXPERIMENTAL RESULTS

Fig. 3.1 depicts schematic view of an AlGaN/GaN HEMT device, having normally-ON characteristics ($V_{th} < 0$), along with all the relevant physical dimensions and stack details. Metal Organic Chemical Vapor Deposition (MOCVD) is used to grown AlGaN/GaN stack on Silicon substrate with the help of AlN nucleation layer. The GaN buffer is grown over a stack of $Al_XGa_{1-X}N$ transition layers. These transition layers are utilized to mitigate dislocation density and to reduce lattice mismatch between GaN buffer and substrate. In order to improve ns.μ product a 1 nm thick AlN spacer layer is employed between AlGaN barrier and GaN buffer [Shen *et al.* 2001b]. A 3 nm thick GaN cap is employed to cover the AlGaN surface. Ni/Au (20/130 nm) metal stack is used to obtain a Schottky gate contact whereas Ti/Al/Ni/Au (20/120/30/50 nm) stack is annealed at 870 °C for 30 seconds to obtain Ohmic contacts. The gate to drain distance (L_{GD}) and gate length (L_G) are 4 μm and 1 μm, respectively, while the device width is 100μm. The measured I_{DS} - V_{DS} characteristics of the device are as shown in Fig. 3.2. The device demonstrated a Hall mobility of 1931 $cm^2/V.s$ with extracted sheet density (n_s) of ~10^{13} cm^{-2}.

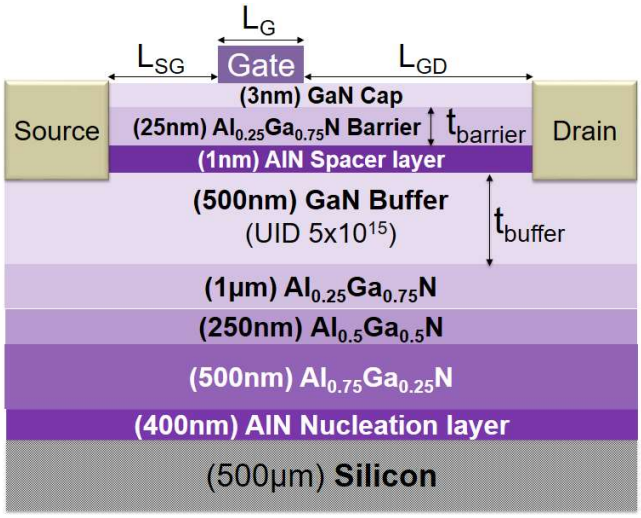


Figure 3.1: Cross-sectional view of the realized HEMT device used for development of a computation strategy to estimate HEMT device performance

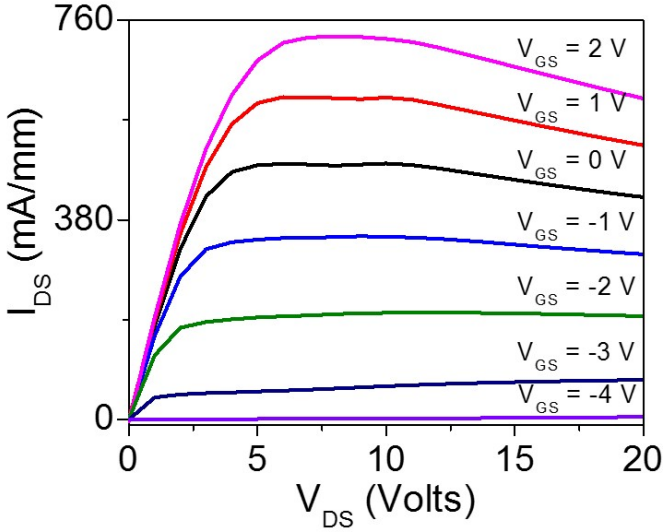


Figure 3.2: Measured I_{DS} - V_{DS} characteristics of the HEMT device for different gate bias voltages. The device considered here is a normally ON device with threshold voltage (V_{TH}) < 0 V.

3.3 COMPUTATIONAL MODELING CHALLENGES: ELECTROSTATICS

3.3.1 Polarization and 2-DEG

Presence of polarization charges in group III-N compounds is well known and owe their presence to absence of inversion symmetry in these compounds. With growth of AlGaN/GaN layers in [0001] direction, polarization charges are stacked in such a manner that an electron channel or 2-DEG is formed in the GaN buffer near the AlGaN/GaN interface. While earlier computation works have modeled polarization charge to estimate 2-DEG density [Karmalkar *et al.* 2001, Meneghesso *et al.* 2004b, Palacios *et al.* 2005, Saito *et al.* 2007, Tirado *et al.* 2007, Faqir *et al.* 2008, Uren *et al.* 2012, Longobardi *et al.* 2014a], however, these works restrict the polarization effect within the AlGaN barrier layer by adding a polarization dipole having a –σ charge at the AlGaN top surface and a +σ charge at the AlGaN/GaN interface. While this approach successfully models current, it neglects polarization charge at any other hetero-material interface. However, as was pointed out in chapter 2, it is essential to encapsulate contribution in polarization field/charge by other epitaxial layers in the device structure to accurately capture their impact on device characteristics. The method discussed here takes care of the polarization charge at all the group III-N interfaces and accounts for parasitic charges as well. Polarization charges are computed numerically according to the procedure suggested by Ambacher *et al*. in [Ambacher *et al.* 1999b], which estimates the polarization charge induced at the interfaces due to gradient in polarization vector at the material interfaces. For a planar device grown in z plane, no polarization charge is expected to be present in the x and y plane due to absence of discontinuity in these directions. However, this assumption might not hold for 3D HEMT devices. The polarization is this present only along the z-plane and can be given as $P_z = P_{strain} + P_{SP}$, where, P_{SP} is the spontaneous polarization and P_{strain} is the piezoelectric polarization given as $P_{strain} = 2.d_{31}.S.(c_{11} + c_{12} - 2c_{13}^2/c_{33})$, d_{31} is piezoelectric coefficient , S is strain in a given layer and c_{ij} are stiffness constant. Quantities c_{ij} & d_{ij} are calculated over the plane at right angle to axis i and are directed along the j direction. For a given epitaxial layer, strain is calculated as $S = (1 - R).(a_0 - a)/a$, where a_0 and a are lattice constants of the unstrained and strained layers respectively and R is a parameter representing strain relaxation. Polarization charge can be calculated from the polarization vector using the relation, $q_{pol} = -A\,\nabla P$, where A is a fitting parameter. In order to capture the electrostatic behavior of the device, the polarization charge thus calculated is included in the Poisson equation ($\nabla\epsilon.\nabla\phi = -q.(p - n + N_D - N_A) + q_{Pol}$).

As the polarization vector is expected to change at all the hetero-material interfaces, this approach is expected to result in polarization charges at all the hetero-material interfaces. While polarization charge at the AlGaN/GaN interface is responsible for inducing charge in 2-DEG channel, its presence at other interfaces is expected to affect vertical field distribution and hence energy band profile in the vertical direction, as depicted in Fig. 3.3(a) and Fig. 3.3(b). The resulting energy band profile results in formation of parasitic hole channels at other material interfaces (Fig. 3.3(c)) and also affects the sheet charge density profile (Fig. 3.3(d)). Figure 3.3(d) further depicts formation of an electron channel in the barrier layer, which is attributed to the energy band profile leading to conduction band energy to be lower than the Fermi energy in the barrier layer (Fig. 3.3(b)). This results in formation of a secondary channel in the device, which is not observed experimentally. These observations and findings clearly justify the significance of accounting for polarization charge at different hetero-material interfaces, for accurately predicting device characteristics. This is also important for making the computational framework adaptive to epitaxial layer arrangement in AlGaN/GaN HEMT device. An accurate estimation of energy band profile in GaN buffer is also significant in evaluating the trap dynamics in the GaN buffer, as the trap energy relative to the conduction band energy can alter the trap occupation probability. Impact of parameter 'A' (in $q_{pol} = -A\,\nabla P$) on n_S is shown in Fig. 3.4(a). As the polarization charge increases with value of 'A', it is reflected in a corresponding increase in n_S. This dependence of n_S & polarization field on value of 'A' is reflected on transfer characteristics of the device, as shown in Fig. 3.4(b). Threshold voltage of the device shows dependence on value

of 'A'. Thus, parameter A can be derived by evaluating its impact on threshold voltage of the device.

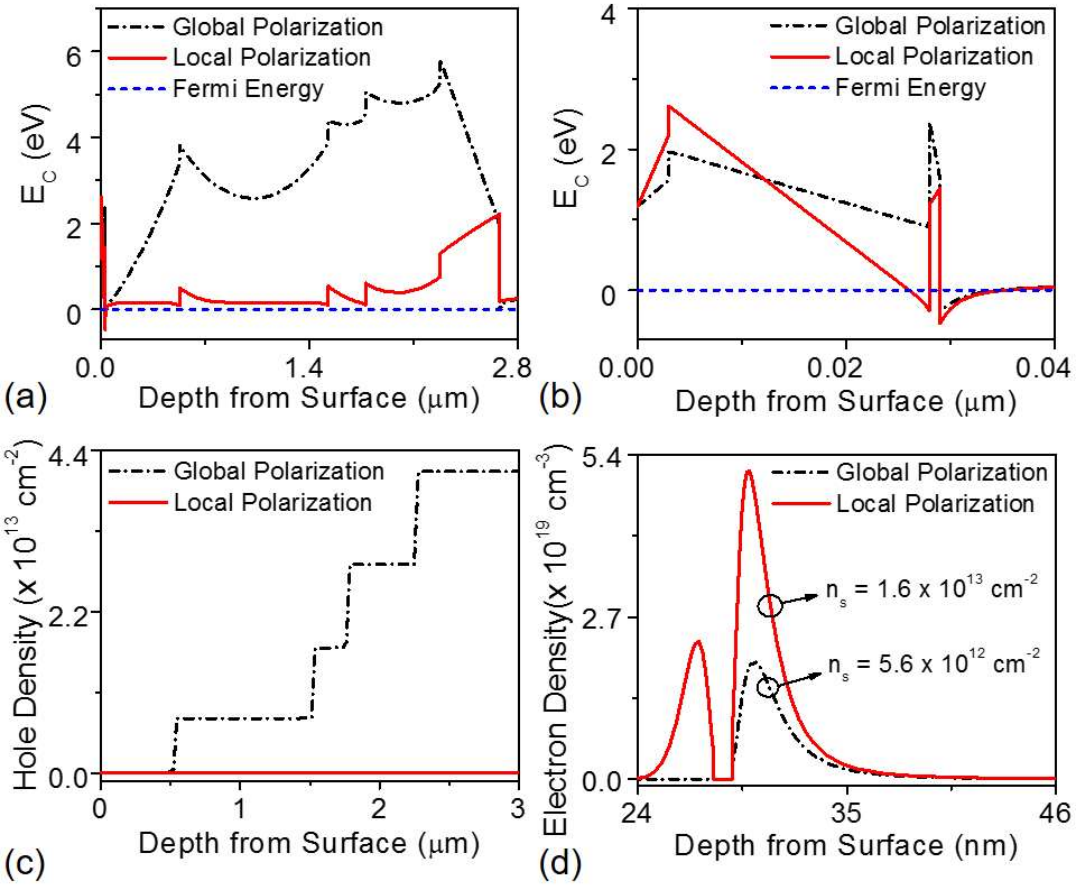


Figure 3.3: Impact of polarization profile on (a) Vertical conduction band energy profile as a function of epitaxial stack depth, (b) Vertical conduction band energy profile near the channel region, (c) Parasitic hole density extracted vertically across the epitaxial stack and (d) electron density profile. The observations are taken on a device in initial rest condition. Integrated values are depicted on the Y-axis of hole density plot, thus presence of a step in the hole density plot indicates a corresponding hole density peak. While the local polarization limits the polarization within the AlGaN barrier layer, global polarization takes into account the polarization charges present at all the hetero-material interfaces within the HEMT device.

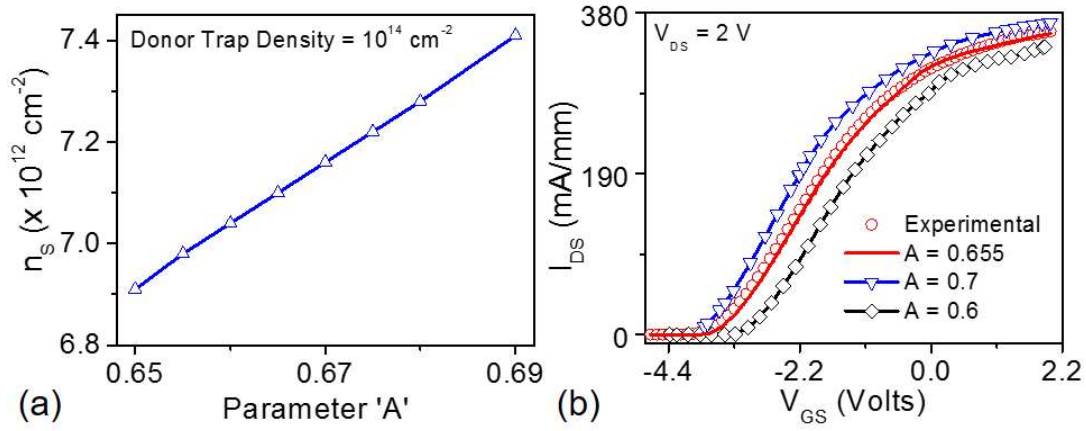


Figure 3.4: Impact of parameter 'A' on (a) 2-DEG charge density, and (b) I_{DS}-V_{GS} characteristics of the device.

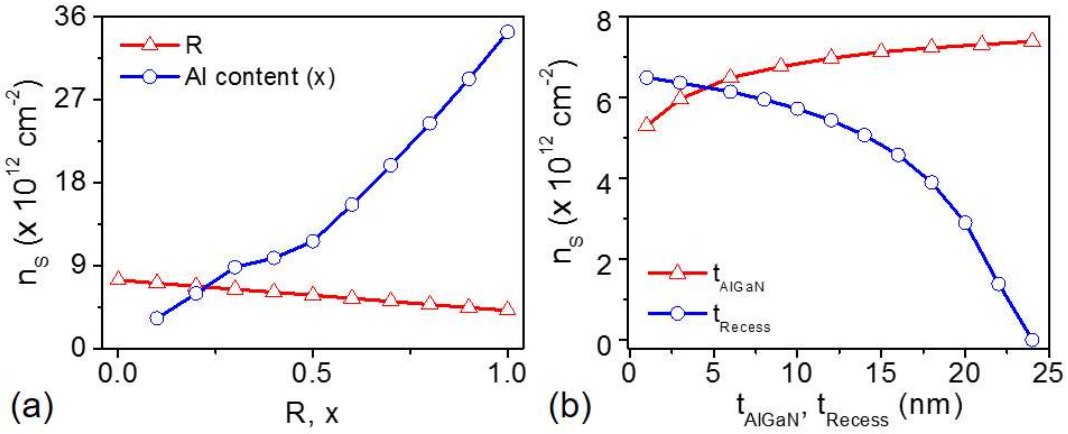


Figure 3.5: Dependence of 2-DEG charge density on (a) Al composition in the $Al_xGa_{1-x}N$ barrier layer and degree of relaxation at the interface between AlGaN barrier and GaN buffer, and (b) thickness of AlGaN barrier and gate-recess depth. For calculations related to relaxation parameter Al mole fraction is assumed to be 0.25 ($Al_{0.25}Ga_{0.75}N$). A 25-nm thick AlGaN barrier is considered for calculations related to gate recess depth, with recess depth calculated from the top of the GaN cap layer. For extracting sheet charge density, a cutline through the epitaxial layers and positioned in the center of gate electrode was considered.

In addition to strain in AlGaN layer, other parameters of the AlGaN barrier, that are known to have an impact on peak carrier concentration and distribution in the channel region, are: Al composition (x) in $Al_xGa_{1-x}N$ barrier layer and thickness of barrier layer (t_{AlGaN}). Bandgap of the barrier layer and the effective polarization at AlGaN/GaN interface increased with an increase in Al composition of the barrier layer. As a result, with an increase in Al composition, n_S increases. However, at higher Al composition ($x > 0.4$) there is relaxation in strain at the interface, resulting in reduced piezoelectric polarization leading to a reduction in value of n_S. All the parameters discussed above, directly or indirectly affect the amount of stress present at the AlGaN/GaN interface and hence affect the sheet charge density. Hence, it is important to incorporate strain/relaxation in the calculations for polarization charge. These are incorporated in the model discussed above for P_{strain} and as strain relaxation parameter S ($S = (1 - R).(a_0 - a)/a$) . Fig. 3.5(a) depicts the modeled and simulated trends. On the other hand, barrier thickness affects polarization field within the AlGaN layer and hence affects n_S. The modeled and simulated trends for n_S dependence on AlGaN barrier thickness and gate recess depth are depicted in Fig. 3.5(b). As can be observed, n_S reduces as the thickness of barrier layer is reduced. This is attributed to channel depletion caused by higher polarization fields in the AlGaN barrier layer. It is important to model this aspect to assist in design of normally-ON devices as well as to design gate recess for normally-OFF devices.

3.3.2 Quantum Effects

Due to formation of a narrow triangle shaped potential well near the AlGaN/GaN interface, quantum confinement effects resulting in reduced density of states and splitting of energy bands are expected to play a key role. It is worth highlighting that most of the simulation studies presented earlier [Karmalkar *et al.* 2001, Meneghesso *et al.* 2004b, Palacios *et al.* 2005, Saito *et al.* 2005, Tirado *et al.* 2007, Bahat-Treidel *et al.* 2008, Faqir *et al.* 2008] have neglected quantum confinement effects. As is depicted in Fig. 3.6 (a), quantum confinement effects result in a reduction in peak 2-DEG concentration value while shifting the peak electron concentration away from the AlGaN/GaN interface. Thus, while the peak concentration value reduces, the electron mobility is expected to improve due to reduced interface scattering. Hence quantum confinement effects are expected to play a key role in accurately predicting electrical parameters such as threshold voltage, trans-conductance and ON-current of the HEMT device. While physically accurate and most sophisticated model to calculate quantum confinement effects is presented by solution of Schrödinger wave equation, for large area HEMT devices it is expected to be

numerically expensive. If properly adopted, quantum approximation models such as density gradient quantum correction model [Ancona *et al.* 1987, Ancona *et al.* 1989], can provide an accuracy comparable to solution of Schrödinger wave equation but at a significantly reduced numerical cost. The model approximates the quantum confinement effects by modifying the classical density formula with introduction of a potential like term Λ_n [Ancona *et al.* 1987, Ancona *et al.* 1989]:

$$n = N_C F_{1/2}\left(\frac{E_{F,n} - E_C - \Lambda_n}{kT_n}\right) \tag{3.1}$$

where, kT_n represents thermal energy of electrons, $E_{F,n}$ is the quasi-Fermi energy for electrons, E_C is the conduction band edge, $F_{1/2}$ is Fermi integral of order ½ and, N_C is the effective density of states. Λ_n is computed as:

$$\Lambda_n = -\frac{\gamma.\hbar^2}{6m_n}.\frac{\nabla^2\sqrt{n}}{\sqrt{n}} \tag{3.2}$$

where, γ is a fitting parameter, $\hbar = h/2\pi$ is Planck's constant, n is electron density and m_n is the electron effective mass.

The electron density profile estimated by solving above equations were in full agreement with solution of Schrödinger wave equation, as shown in Fig.3.6 (a), for value of γ as 2.2 and 1.3 for AlN and GaN, respectively. A comparison of transfer characteristics of the device calculated considering quantum corrections with that of the calculation with classical equations, as shown in Fig. 3.6(b), interestingly indicates almost similar characteristics. This in turn is attributed to compensation of reduction in n_S by an increase in value of μ, resulting in a constant $n_S.\mu$ product.

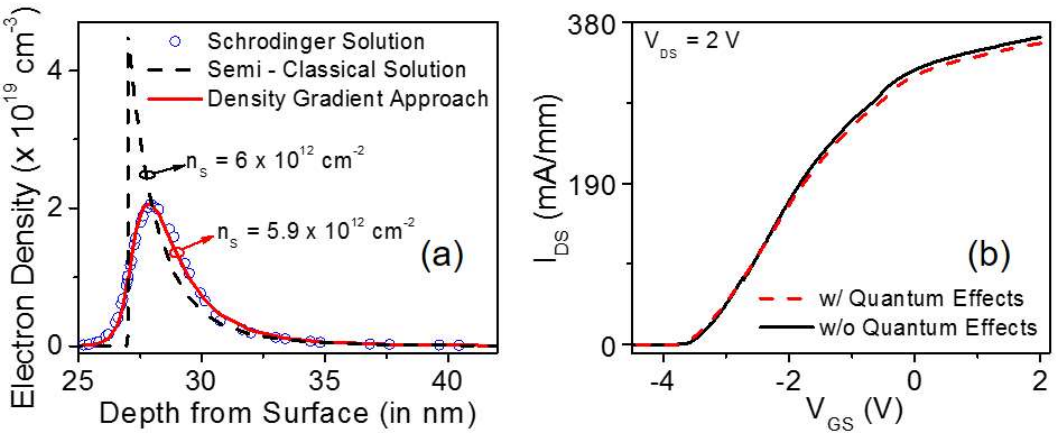


Figure 3.6: (a) A comparison of sheet charge density profile extracted using semi-classical equation with that of the solution obtained by taking quantum confinement effects into account. (b) Transfer characteristics of the device under influence of quantum effects and without it.

3.3.3 Surface Traps

While presence of polarization in GaN is considered as the primary source of 2-DEG, however, Ibbetson *et al* in [Ibbetson *et al.* 2000] proposed that polarization charges alone are not sufficient to explain 2-DEG charge density in AlGaN/GaN HEMT devices which exists even in absence of intentional doping in AlGaN barrier layer. In fact, the surface dependent characteristics of AlGaN/GaN HEMTs, like mitigation of DC/RF dispersion [Green *et al.* 2000, Chung *et al.* 2009], gate and drain lag effects [Meneghesso *et al.* 2004b, Tirado *et al.* 2007] by surface passivation suggests presence of surface traps [Bisi *et al.* 2013], which in turn significantly affects

the 2-DEG charge density. Ibbetson *et al* further suggested surface donor traps to be responsible for charge carriers in the 2-DEG channel, and in absence of surface traps, a hole gas should exist on device to result in an electron channel at the AlGaN/GaN interface [Ibbetson *et al*. 2000]. Alternatively, Meneghesso *et al* proposed (i) formation of a hole populated layer on the device surface to balance the electrons in the 2-DEG channel thereby maintaining the charge neutrality condition, and (ii) the dangling bonds representing surface states behave as trap sites to capture these holes [Meneghesso *et al.* 2004b]. For analyzing true nature of surface traps simulations were done initially with ideal surface, thereby neglecting presence of any surface traps. Fig. 3.7(a) depicts the simulation results which reveal a surge in drain current, which now increases with drain voltage and doesn't saturate. As is shown in Fig. 3.7(a), this surge in drain current is caused by an increase in the hole current, whereas the electron current saturates. The electron current in this case is carried by the 2-DEG channel whereas the hole current is carried by the hole gas present on surface. As the experimental device characteristics, as shown in Fig. 3.1(a), don't show such a surge in output current, it can be conclusively said that surface hole current is absent in the practical AlGaN/GaN HEMTs. This in turn requires compensation of holes present on device surface by some means. Fig. 3.7(b) shows output characteristics of device in presence of donor type surface traps, and as can be observed the hole current is co0mpletely suppressed and the device output characteristics now show a HEMT like feature where drain current initially increases linearly and then saturates with a further increase in drain voltage. This observation is in agreement with the earlier theory by Meneghesso *et al* [Meneghesso *et al*. 2004b]. Fig. 3.7(c) and Fig. 3.7(d), which depict impact of surface trap density and energy on 2-DEG density respectively, further quantify the argument that 2-DEG charge density is a strong function of surface traps.

Since ionized surface traps will introduce positive charge in the system, an equal increase in the 2-DEG charge proportional to ionized surface trap density is expected to compensate the positive charge sheet at the surface.

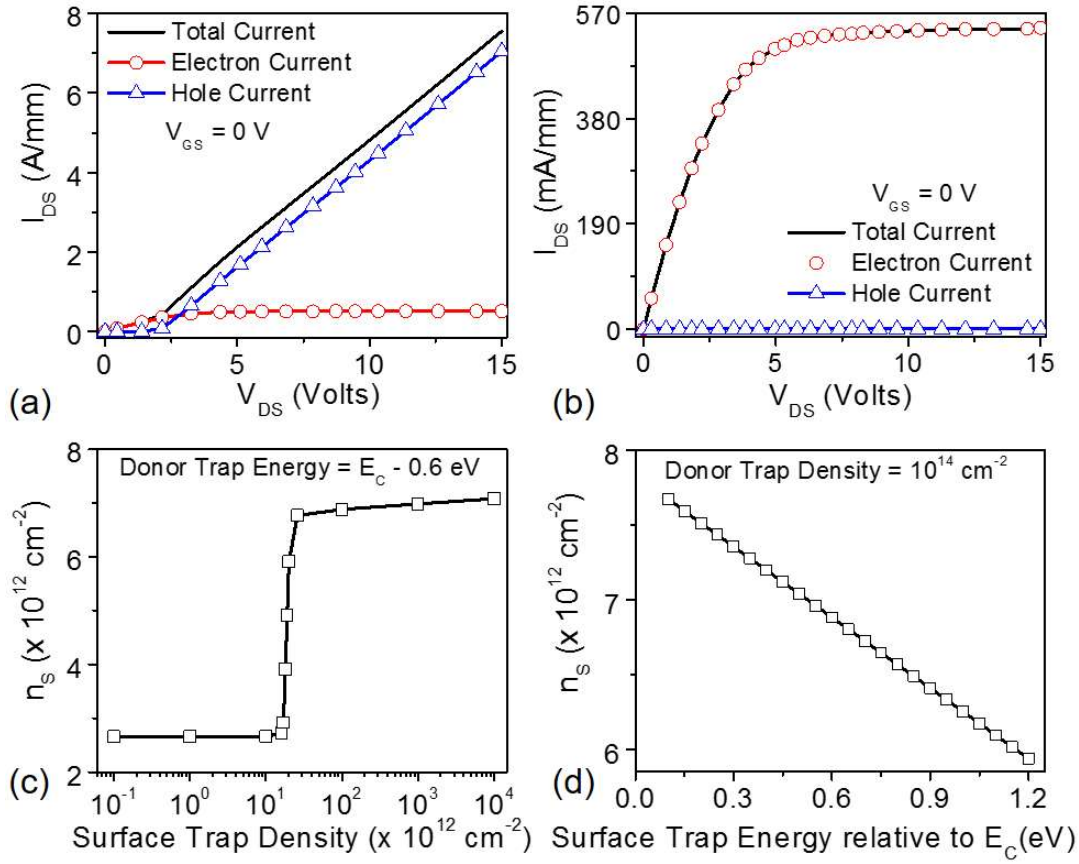


Figure 3.7: Device's output characteristics (a) with ideal surface and (b) with donor traps on device surface (Density = 1 x 10^{14} cm^{-2} and Energy = E_C – 0.6 eV). Sheet charge density extracted as a function of parameters of donor traps on device surface: (c) Density, and (d) Energy of surface traps.

However, as observed from Fig. 3.7(c), the 2-DEG density increases at a slower rate with surface trap density and shows an abrupt increase beyond a particular threshold value of surface trap density. The initial donor trap concentration is ionized by the hole gas present on the surface and hence their contribution to the 2-DEG charge is negligible. However, as the surface donor trap concentration is further increased, they ionize in presence of strong polarization fields and donate their electron to the 2-DEG channel resulting in an increase in 2-DEG density.

However, as the surface trap density is increased beyond a certain value, n_S saturates. This is attributed to Fermi level pinning at the device surface which restricts ionization of surface donor traps, which are now not able to transfer their electron to 2-DEG channel [Longobardi *et al.* 2014b]. The above argument is further quantified in Fig. 3.7(d), which depicts that the 2-DEG density further increases as the trap energy level is brought closer to the conduction band edge, thereby increasing ionization of surface traps. From above discussion, it can be concluded that surface traps and polarization charge control the sheet charge density and hence are important parameters to model the device characteristics. While threshold voltage of the device shows dependence on polarization charge, gate leakage current is a function of surface trap parameters and will be discussed on following sections.

3.3.4 Traps

Owing to the growth conditions, HEMT devices are prone to bulk as well as interface traps. These trap sites can arise from the defects or impurity atoms introduced in the material during growth process. Depending on the physical location, these trap sites can be either donor or acceptor in nature. However, the spatial and energy distribution of these traps and their correlation with the growth parameters is not very well understood. Based on the impact of these traps in reliability aspects and 2-DEG channel, as discussed in chapter 2, earlier works suggest presence of acceptor traps in the bulk of GaN cap, AlGaN barrier and GaN buffer whereas donor type traps are expected to be present on the device surface [Faqir *et al.* 2008]. While traps can be present at different locations in the device, due to their more pronounced impact on device channel, traps on the device surface and those in the GaN buffer are expected to have dominant impact on device characteristics. In order to establish relevance of these traps in modeling the device behavior, donor traps on GaN cap surface and acceptor traps in GaN buffer are considered here. While the impact of surface traps was discussed in detail in the earlier sections, bulk traps in GaN buffer along with its impact on device characteristics is discussed in this section.

In DC characteristics of AlGaN/GaN HEMTs, buffer traps are often associated with Negative Differential Resistance (NDR). NDR is commonly observed in output characteristics of AlGaN/GaN HEMTs, where after saturating the drain current starts reducing gradually as drain voltage is stressed above a certain threshold value (V_{DS} > 10 V in this case). In order to evaluate impact of traps in GaN buffer on device characteristics, acceptor type traps were considered in the GaN buffer with a Gaussian like spatial distribution. Peak of this trap distribution was taken near the AlGaN/AlN interface and was considered to be spread up to the channel region, as depicted in Fig. 3.8(a). This type of a trap distribution better estimates the traps introduced by defects/dislocations in the GaN buffer having maximum density near the interface with AlN nucleation layer while the channel region is almost defect free. As the objective here is to investigate impact of defects/dislocations induced traps on device characteristics, traps induced by compensation doping were neglected. The traps were considered at an energy level of E_C - 0.96 eV, which is associated with the activation energy of dislocations in GaN devices [Bisi *et al.* 2013]. Fig. 3.8(b) depicts the impact of this trap profile on output characteristics of the device. Three different buffer trap profiles were considered here to analyze the impact of increase in trap concentration in the bulk (peak value) as well as near the channel region (spread of the trap profile). It can be observed that the magnitude of reduction in current in the NDR region is independent of the trap profile, whereas the saturation current reduces as trap concentration is increased in the proximity of the GaN channel. Thus, it can be fairly concluded that buffer traps are not the source of NDR effect observed in output characteristics of the device but increase in

buffer trap concentration results in a reduction in the saturation current, which in turn can be attributed to reduction in carrier density in the channel region.

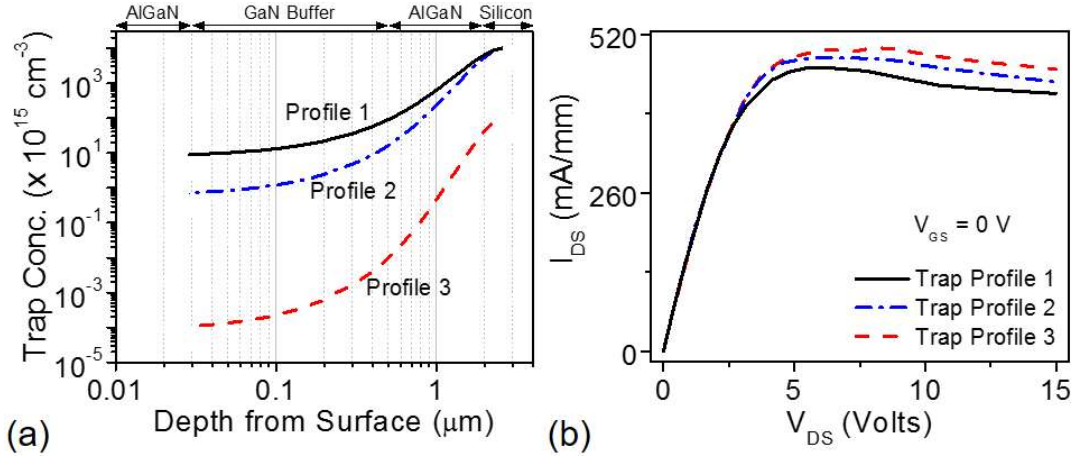


Figure 3.8: (a) Acceptor trap profile, approximated by Gaussian function, assumed to be present in the GaN buffer of AlGaN/GaN HEMT device. (b) Impact of the assumed trap profiles on output characteristics of the device. Acceptor type buffer traps are assumed as deep level traps with an activation energy of E_C - 0.96 eV.

For sake of completeness, the trap energy was swept in the range of E_C - 0.5 eV to E_C - 2.9 eV to take into account the sources of compensating doping, taking into consideration the energy level for C (E_C - 2.5 eV) [Verzellesi *et al.* 2014b] as well as Fe (E_C - 0.5 eV) [Uren *et al.* 2012]. Even with a variation in trap energy the results showed a similar trend, with an increase in trap concentration near the channel region leading to reduced saturation current of the device. This further agrees with the argument that buffer traps are not the source of NDR phenomena but have a significant influence on n_S and saturation current of the AlGaN/GaN HEMT device. Hence NDR depicted in output characteristics of the device originates from some other physical mechanism and will be discussed in later sections. It is important to mention that effect of traps on device characteristics can be truly captured only if hot electrons are considered along with traps, so as to account for modified trap dynamics under presence of hot electrons. Unlike previous works [Wang *et al.* 2012], we have for the first-time modeled effect of carrier heating in combination with surface and bulk traps. Details on carrier dynamics and model to account for hot electrons is discussed in later section.

3.3.5 S/D Contacts

As explained in section 3.2, S/D contacts were realized using a well-established metal stack (Ti/Al/Ni/Au). The contact deposition process involves a high temperature post deposition anneal to allow the metal layers to diffuse deep down into GaN buffer so as to make contact with 2-DEG, as shown in Fig. 3.1. Annealing results in formation of TiN allow due to Ti present at the bottom. This alloy formation is known to create N vacancies in GaN. Formation of TiN alloy results in lowering of the barrier height at the contact to 2-DEG interface and the N vacancies enhance tunneling [Fan *et al.* 1996], leading to an Ohmic contact. In order to model the contact behavior, S/D contacts were taken as metals with work function equivalent to that of TiN (~4.1 eV) and was considered to have a diffusion depth of ~2 nm below the 2-DEG. Further, to capture the effect of donor/N vacancies, a thin n-type doped region was considered at the metal-semiconductor interface in the proximity of S-D contacts. Finally, equations pertaining to Schottky interface were solved to account for tunneling nature of carrier transport between S/D contacts and 2-DEG channel. In addition to this, the Schottky contact was connected with a lumped resistance in series. The impact of this lumped resistance on the electrical characteristics of HEMT device is depicted in Fig. 3.9. It is worthwhile to note that the contact behavior is

different from that of an ohmic contact, as the contact resistance in this case affects the linear as well as saturation drain current. Above findings and discussions also highlight the relevance of physics-based modeling of contact behavior in AlGaN/GaN HEMTs to have a reasonable estimate of the device characteristics.

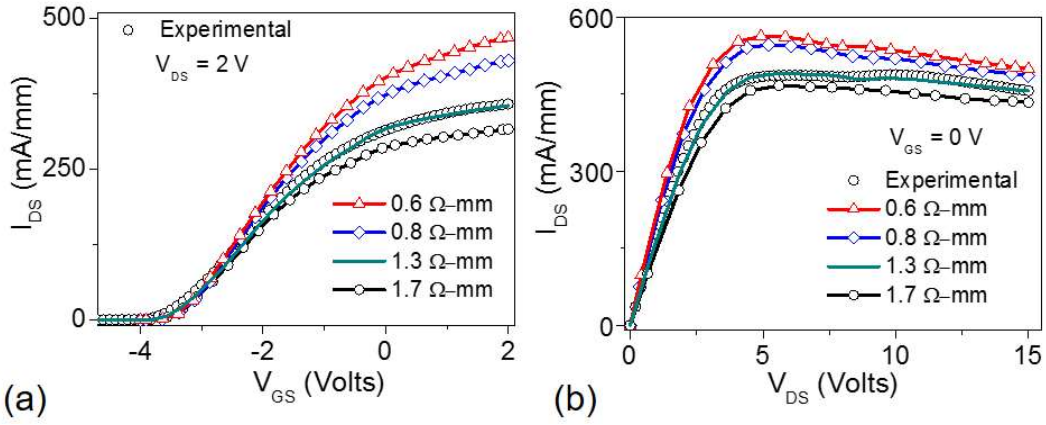


Figure 3.9: Impact of Source/Drain contact resistance on (a) transfer and (b) output characteristics of the HEMT device. An agreement between the simulation and experimental results can be observed for the contact resistance value of 1.3 Ω.mm.

3.4 COMPUTATIONAL CHALLENGES & MODELING: CARRIER DYNAMICS AND TRANSPORT

Modeling of different electrostatic aspects of AlGaN/GaN HEMTs was discussed in previous section. This section further extends the discussion to include carrier dynamics and transport taking into account aspects like mobility, high field effects, self-heating and hot carriers.

3.4.1 Carrier Transport

Carrier mobility is often used to capture the dynamics of carrier transport in semi-classical systems. Depending on the device structure and material used, carrier mobility is governed by a combination of several different scattering mechanisms. For AlGaN/GaN based HEMT devices, the major scattering mechanisms are classified as acoustic phonon scattering, ionized impurity scattering, non-polar and polar optical phonon scattering, alloy scattering, and piezoelectric scattering [Zanato *et al.* 2004, Knap *et al.* 2005, Lisesivdin *et al.* 2007, Tülek *et al.* 2009, Celik *et al.* 2012]. For AlGaN/GaN HEMTs, optical phonon scattering is known to be the dominant scattering mechanism at room temperature [Hsu *et al.* 1997, Fang *et al.* 2012]. Here the carrier mobility under influence of these effects is calculated using the models and transport parameters for GaN proposed by Arora *et al* in [Arora *et al.* 1982] and Farahmand *et al* in [Farahmand *et al.* 2001], respectively. Low field mobility is reasonably approximated by the model adopted from [Arora *et al.* 1982], described by numerical equation as follows:

$$\mu_0(T,N) = \mu_{min}\left(\frac{T}{300}\right)^{\beta_1} + \frac{(\mu_{max}-\mu_{min})\left(\frac{T}{300}\right)^{\beta_2}}{1+\left[\frac{N}{N_{ref}\left(\frac{T}{300}\right)^{\beta_3}}\right]^{\alpha(T/300)\beta_4}} \tag{3.3}$$

Here T and N are the lattice temperature and total doping density respectively, N_{ref} denoted the reference concentration and takes into account the mobility degradation at higher concentrations, , μ_{max} & μ_{min} are the maximum and minimum expected mobility values, α is an exponential factor & controls slope around N = N_{ref} , and β_1, β_2, β_3 & β_4 account for the temperature dependence of

minimum expected mobility, lattice scattering, ionized impurity scattering and concentration dependent mobility, respectively. The values of these material dependent parameters was extracted using Monte Carlo simulations by Farahmand *et al* in [Farahmand *et al.* 2001] and reasonably approximates the experimentally observed mobility values. Hence, the parameter values were adopted from [Farahmand *et al.* 2001] to model carrier transport.

While at lower electric fields the accelerated electrons thermalize as a result of optical phonon scattering, however, with increase in electric field other scattering mechanisms start to dominate the carrier mobility. For AlGaN/GaN HEMT devices, carrier transport at higher values of electric field is governed by inter valley scattering [Abou El-Ela *et al.* 2013]. At higher electric field values, the electrons gain sufficient energy to transfer to higher energy conduction band valley. This inter valley transfer results in the transferred electrons with increased effective mass and hence reduced carrier mobility and velocity. As a result of inter valley scattering, a negative differential mobility is observed at higher electric field values. This reduction in mobility continues till all the states in the upper valley are occupied. As the electrons can now no longer jump to higher energy sub-band, the electron mobility now saturates and remains constant with further increase in electric field. This behavior was modeled by Farahmand et al. [Farahmand *et al*. 2001]. This work adopts a similar model and adopts the model parameters values as extracted from Monte Carlo simulations in [Farahmand *et al*. 2001]:

$$\mu = \frac{(\mu_0(T,N)+v_{sat}\cdot\frac{E^{n_1-1}}{E_C^{n_1}}}{1+a\left(\frac{E}{E_C}\right)^{n_2}+\left(\frac{E}{E_C}\right)^{n_1}} \tag{3.4}$$

where μ_0 is the low field mobility approximated by eq. 3.3, v_{sat} is the saturated velocity, E_C is the critical electric field required for electron transfer, n_1, n_2 & α are fitting parameters extracted using Monte Carlo simulations. The electrical characteristics as shown in Fig. 3.10 depict a dramatic reduction in drain current as the higher electric field induced mobility degradation is taken into account. It is worth mentioning that as the 2-DEG channel is located at a distance from the AlGaN/GaN interface, owing to quantum confinement, the normal electric field has a negligible impact on channel mobility or carrier transport. While the above-mentioned model reasonably estimates the channel mobility, however, to account for velocity overshoot effect, carrier energy needs to be modeled and affects the device characteristics, as will be explained in later sections.

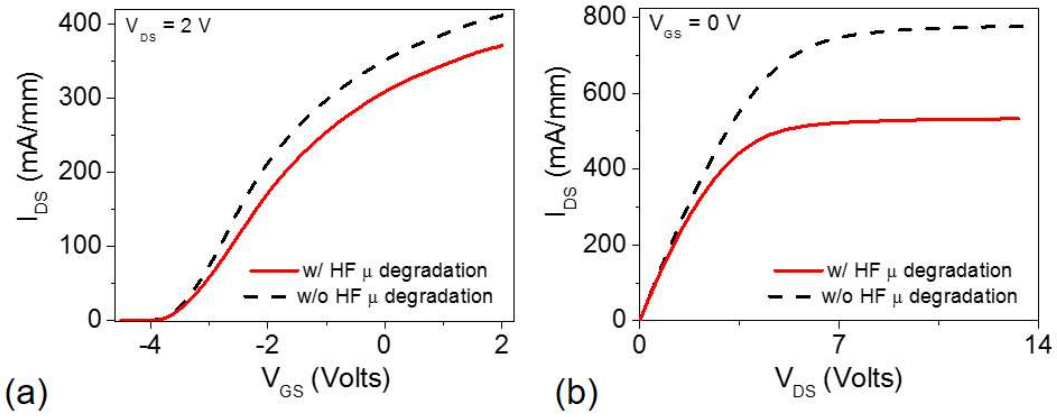


Figure 3.10: Effect of mobility degradation observed at higher electric fields on (a) transfer and (b) output characteristics of the HEMT device.

3.4.2 Gate Stack Modeling

Besides computing leakage through GaN buffer, modeling gate leakage is equally significant in evaluating reliability of AlGaN/GaN HEMTs and predicting effects caused by interaction of gate electrode with traps, like DC-RF dispersion, gate and drain lag etc. Here we have considered a Schottky type gate contact as modeling leakage through Schottky gate is more complex and non-trivial as compared to HEMT devices with Metal-Insulator-Semiconductor (MIS) topology at gate electrode. For Schottky gated device, with gate biased in the reverse condition, earlier works suggest Fowler Nordheim (FN) tunneling along with Poole-Frenkel emission to be the primary source of leakage current [Turuvekere *et al.* 2014]. On the other hand, leakage current in forward bias condition is caused by thermionic emission. In addition to above mentioned mechanisms, we for the first time have taken into account the electrical coupling between gate and 2-DEG channel, which we found to be a significant source of gate current in the forward bias condition.

Tunneling effects were accounted with the help of non-local tunneling at the gate electrode. Nonlocal tunneling is discussed in detail by Ieong et al. in [Ieong *et al.* 1998], and used WKB approximation to calculate tunneling probability. Nonlocal tunneling considered here, as explained in [Synopsys 2014], considers the dependence of tunneling current on energy band profile along the complete tunneling path. In addition to this, impact of traps present on device surface and in electrical contact with gate electrode is also modeled in this work, which can alter the surface potential and can affect tunneling probability or provide additional leakage paths for the gate current. While presence of traps on device surface has been taken into account in several earlier works [Meneghesso *et al.* 2004b, Palacios *et al.* 2005, Tirado *et al.* 2007, Faqir *et al.* 2008, Medjdoub *et al.* 2008], however they were modeled using a surface trap parameters with fixed density and energy, without evaluating their influence on gate leakage. Saito *et al* in [Saito *et al.* 2005] have considered impact of traps on device surface on the gate leakage current, however, the traps were modeled as fixed defect charge and accounted for impact only on the Schottky barrier height. These approaches essentially neglect the important phenomena of trapping/de-trapping associated with the presence of surface traps. Impact of surface trap parameters on gate leakage is studied and presented for the first time in this work and is as depicted in Fig. 3.11(a) and (b). Figure 3.11(a) and (b) suggests that gate leakage is significantly influenced by surface traps, with an increase in gate leakage as the difference between trap energy level and conduction band energy reduces and/or when there is an increase in trap density. This dependence of gate leakage on surface trap density can be explained by considering energy bands under influence of positively ionized surface donor traps, as depicted in Fig. 3.11(c). Positive charge contributed by surface traps in ionized state results in band bending near the gate edge. This significantly reduces the tunneling barrier leading to an exponential increase in gate leakage current. It is worth highlighting that as the traps are not present under the gate electrode this phenomenon will predominantly result in a higher current through gate edges. As surface trap energy level is moved closer to E_C, there is an increased probability of ionization of donor type surface traps resulting in an increase in tunneling current (Fig. 3.11(b)). A surface trap density of 2.39×10^{13} cm^{-2} with an activation energy of E_C - 0.15 eV was able to reproduce the gate leakage characteristics for the device realized in this work. A different surface trap density of 1×10^{14} cm^{-2} located at an energy level of E_C-0.6 eV was assumed in section 3.2.3. The reason was to select an energy level corresponding to N vacancy in GaN [Bisi *et al.* 2013], as it was more likely to be present. However, traps located as such deep energy levels were unable to explain the experimentally observed gate leakage characteristics. On the other hand, the derived trap energy level of E_C - 0.15 eV is closely related to energy level of surface states in n-GaN (E_C - 0.12 eV) [Bisi *et al.* 2013]. It is worth mentioning that this change in trap parameters does not cause any significant deviation in the DC characteristics of the device.

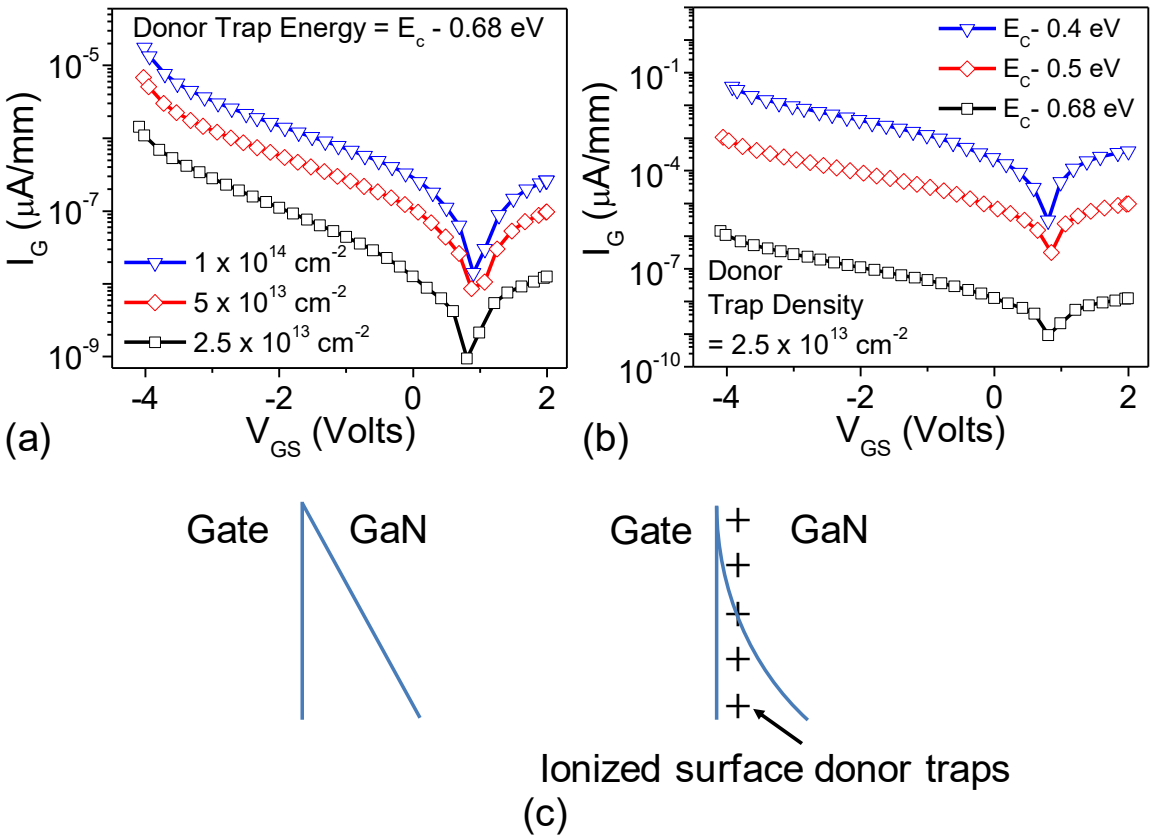


Figure 3.11: Dependence of gate leakage characteristics on the surface trap (a) density and (b) energy. The surface trap energy depicted here is calculated with respect to the conduction band energy (E_C). (c) Bending of energy bands near the gate electrode under influence of ionized surface donor traps leading to enhanced tunneling.

As shown in Fig. 3.12(b), with proper modeling of surface traps and tunneling current an excellent agreement with the measured gate leakage characteristics can be observed, except for $V_{GS} > 0.8$. With a positive bias applied on gate the electrons should now be transported into the gate by thermionic emission or tunneling. However, presence of surface states depletes the thin GaN cap layer of any free charge carriers, resulting in a lower leakage current in the forward direction as compared to the reverse leakage current through the gate terminal. As a result, the thermionic emission from GaN cap to gate electrode results in a lower current than what is experimentally observed, suggesting at a different leakage path or mechanism which can result from the device geometry and gate topology. A closer look to the device geometry in this case reveals a coupling between the gate metal and 2-DEG channel, depicted in Fig. 3.12(a). As the gate metal over GaN cap is extended up to the gate pad, it comes in contact with the 2-DEG channel as it crosses over the MESA region, resulting in a physical contact between the gate metal and 2-DEG channel.

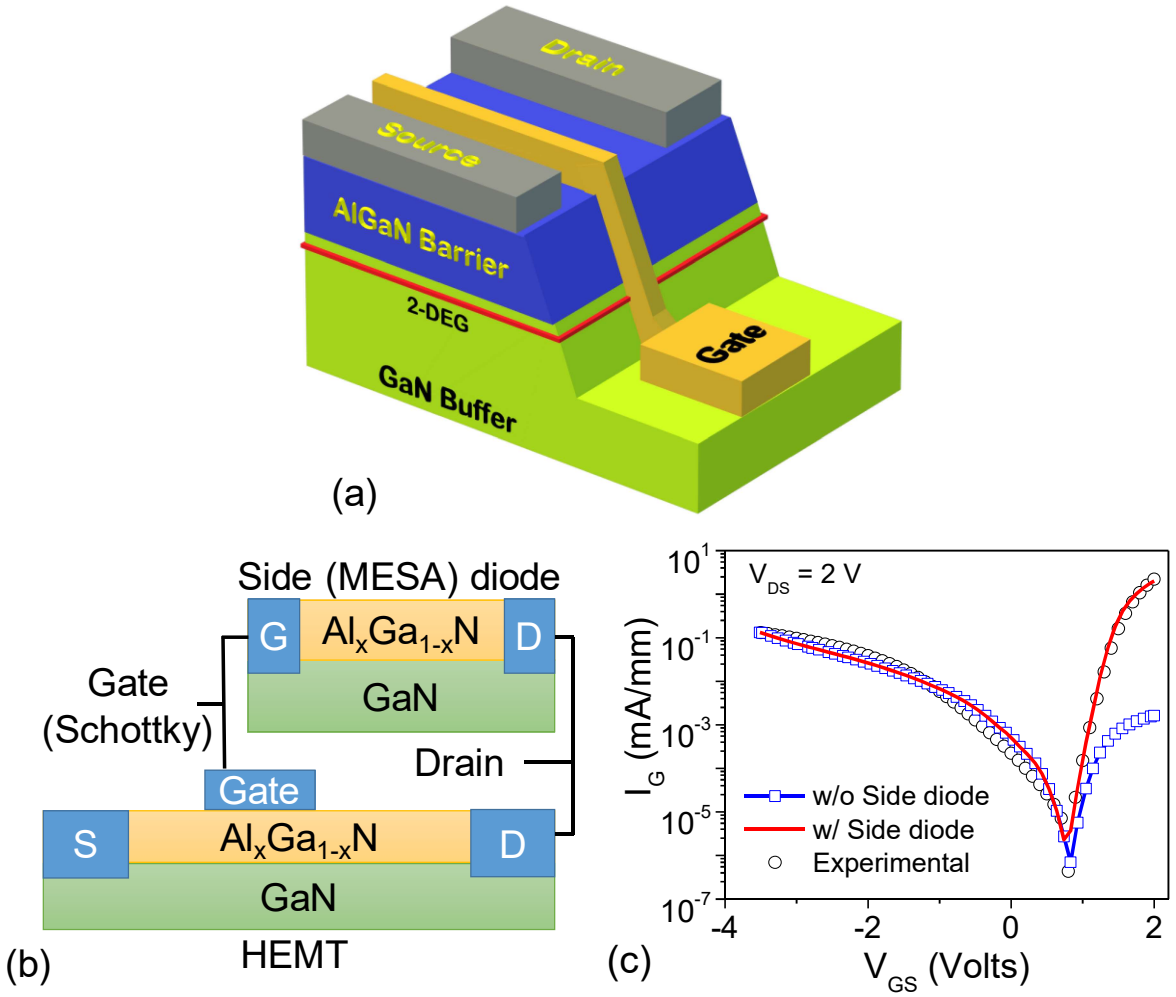


Figure 3.12: (a) 3-D representation of a conventional AlGaN/GaN HEMT structure depicting contact between the gate finger and 2-DEG in the MESA region resulting in formation of side diode. (b) The HEMT structure simulated in parallel with the side (MESA) diode between Schottky gate and drain contact. This structure is considered to take into account the MESA gate leakage component for positive gate bias voltages. (c) Computed gate leakage characteristics for the combined HEMT device and side diode structure compared against the experimental characteristics. Experimental devices had a $100\mu m \times 1\mu m$ gate finger. An excellent agreement with the experimental characteristics can be observed for devices where MESA leakage component was considered. A surface trap density of 2.39 x 10^{13} cm^{-2} with activation energy of E_C - 0.15 eV is considered.

As a result of this direct coupling between gate metal and 2-DEG channel there is a reduction in built-in potential necessary for the side (MESA) diode to start conducting [Lee *et al.* 2013]. This leads to an early increase in forward leakage current. Mixed mode simulations were conducted with MESA diode connected in parallel to gate and drain terminal1 of the HEMT device, as shown in Fig. 3.12(a), to take into account the gate leakage component through the MESA diode. The leakage characteristics obtained from this mixed mode simulation, as shown in Fig. 3.12(b), reveals that the proposed extension for modeling gate leakage behavior successfully reproduces the gate leakage characteristics of the device which are in an excellent agreement with the experimental characteristics. It is worth mentioning that the MESA diode exhibited a Schottky barrier height which was ~0.75 eV higher as compared to Schottky barrier height of HEMT's gate electrode. This could be attributed to slanted MESA trench profile and trap states present at the gate/2-DEG interface.

3.4.3 Lattice and Carrier Heating: Impact on Carrier Transport

As the GaN HEMT devices are expected to operate at high power densities and are required to carry high electric currents, a significant device heating is expected to be present. Hot spots can build up in absence of proper heat removal from the system and can have an observable impact on device performance. This necessitates physics-based modeling of lattice heating with suitable thermal boundary conditions. Here lattice heating and its impact on carrier transport are accounted using the numerical method proposed by Wachutka *et al* in [Wachutka 1989] [Wachutka 1990]. In addition to this, the device operation at higher electric fields also makes it necessary to consider generation of hot electrons in the system. These highly energized electrons can alter the trap occupation dynamics and can also result in generation of new traps. On the other hand, the kinetic energy gained by these electrons also results in velocity overshoot effect which improves carrier transport. As any variation in the occupation dynamics of surface and/or buffer traps is directly reflected in the 2-DEG density, it is important to consider the generation of hot electrons in presence of traps in the device. While hot electrons were considered by Wang *et al* in [Wang *et al.* 2012], however, its role in combination with surface and bulk buffer traps while considering lattice heating was never given importance before.

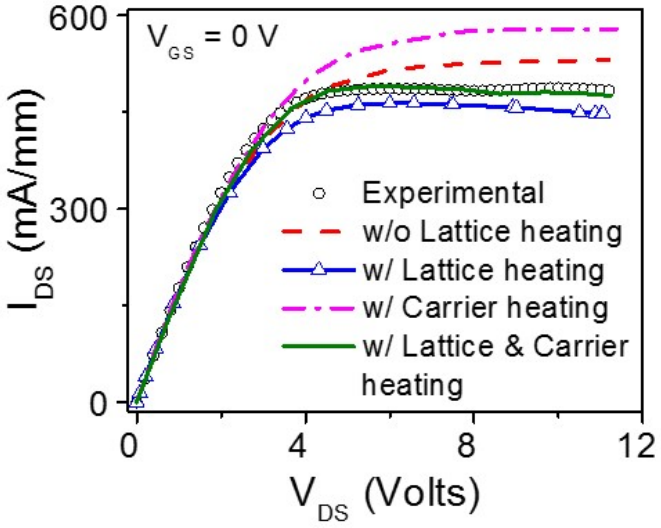


Figure 3.13: A comparison of the computed output characteristics of the device with experimentally extracted output characteristics. Impact of lattice and carrier heating is depicted in the figure to highlight significance of including lattice and carrier temperature in the device computations.

Here the carrier transport in presence of hot electrons with temperature (T_n) was modeled according to the carrier transport model proposed by Stratton *et al* [Stratton 1962] and improvised by Apanovich *et al* [Apanovich *et al.* 1995]:

$$\overrightarrow{J_n} = \mu_n(n\nabla E_C + kT_n\nabla n - nkT_n\nabla ln\gamma_n - 1.5nkT_n\nabla lnm_n) \tag{3.5}$$

Here $\gamma_n = \left(\frac{n}{N_C}\right)\exp\left(-\frac{E_F,n-E_C}{kT}\right)$, m_p and m_n represent effective masses of holes and electrons, respectively and N_C represents the effective density of states. Finally, the effect of carrier energy on mobility is captured by replacing electric field (E) in eq. 3.4 by [Apanovich *et al.* 1995]:

$$E = \sqrt{\frac{\max(E_n - E_0, 0)}{\tau_{e,n} q \mu_n}} \tag{3.6}$$

where $E_0 = 3kT/2$ represents the equilibrium thermal energy, $E_n = 3kT_n/2$ represents the average electron energy, and $\tau_{e,n}$ represents the energy relaxation time.

As shown in Fig.3.13, inclusion of lattice and carrier heating has a significant impact on the device characteristics. Neglecting the lattice heating while accounting for carrier heating results in an over-estimation of device current. On the other hand, taking lattice heating into account without considering the carrier heating leads to an under-estimation of device current. In addition to this, it can be observed that NDR phenomena can be seen in the output characteristics only if lattice heating is considered. This suggests that lattice heating is the source of NDR observed in HEMT characteristics. An excellent agreement with experimental data is observed only if both lattice & carrier heating are simultaneously taken into account while calculating the HEMT device characteristics. While lattice heating takes into account the negative impact of lattice heating on device performance, carrier heating is required to account for velocity overshoot effect resulting in an increase in output current.

3.5 CONCLUSION

DC characteristics of AlGaN/GaN HEMT devices were successfully modeled to be in excellent agreement with the experimental device behavior. Several different physical parameters were analyzed and their relevance in estimating the device performance was established with associated physics. It was shown that the presence of polarization charges across different hetero-epitaxial interfaces significantly affects the conduction band energy profile, resulting in accumulation of parasitic charges, besides resulting in formation of a sheet charge density. These observations justify the significance inclusion of polarization charge at all hetero-material interfaces, which was ignored in previous works. The impact of surface traps on the sheet charge density, and device characteristics was extensively studied and presented along with its impact on gate leakage characteristics for the very first time. In addition to this, gate leakage was proposed as a tool to determine surface trap parameters like density and energy. The difference in experimental and modeled gate leakage characteristics helped to identify the additional leakage sources contributing to gate current. In the devices considered here, direct electrical coupling between Schottky gate electrode and 2-DEG channel in the MESA region was found to be the source of additional leakage path adding to gate leakage current. Instead of being modeled as ohmic contacts, the Source/Drain contacts were modeled with the help of using a Schottky interface taking into account the tunneling nature of carrier transport between S/D contact and the 2-DEG channel. The contact resistance was found to affect the linear as well as saturation characteristics, suggesting that modeling of contacts as fixed ohmic contacts can give misleading results for AlGaN/GaN HEMTs. These observations highlight the importance of physics-based modeling of S/D contact interface with the 2-DEG channel to accurately predict device behavior. The NDR phenomena observed in output characteristics of the device was found to be caused by self-heating of the device, while buffer traps had negligible contribution. Finally, it was found that it is equally important to consider lattice heating as well as carrier heating to have an estimate of the AlGaN/GaN HEMT device performance.

…